Dyes and Pigments xxx (xxxx) 111116

Contents lists available at ScienceDirect

Dyes and Pigments

journal homepage: www.elsevier.com/locate/dyepig

Indirubin: Nature finding efficient light-activated protective molecular mechanisms

Danîela C. Nobre [a], Estefanía Delgado-Pinar [a], Carla Cunha [a], Adelino M. Galvão [b], J.Sérgio Seixas de Melo [a, 1, *]

[a] University of Coimbra, CQC-ISM, Department of Chemistry, Rua Larga, 3004-535, Coimbra, Portugal
[b] Centro de Química Estrutural, Institute of Molecular Sciences, Instituto Superior Técnico, Universidade de Lisboa, Av. Rovisco Pais, 1049 001, Lisboa, Portugal

ARTICLE INFO

Keywords:
Indirubin
Indigo
H-chromophore
Indirubin derivatives
TDDFT
Photochemistry
Ultrafast spectroscopy
Proton transfer
Keto
Enol
Syn-rotamer

ABSTRACT

Indirubin (**INR**), a red structural isomer of the blue indigo (**IND**) shows, for an organic dye, a high stability towards light. The nature of this photostability is unknown and is here proposed to be linked to efficient dark processes dominating the excited state deactivation. As with **IND**, an excited state proton transfer (ESPT) process, together with the possibility of rotation around the central carbon-carbon bond (with formation of a *syn*-rotamer), are solvent dependent, active molecular mechanisms of the decay pathways in **INR**. To equate this behaviour, **INR**, together with *N*-methyl-(**MINR**) and *N,N′*-dimethyl-indirubin (**DMINR**) have been synthetized and fully investigated from a combination of steady-state, fast-transient absorption and fluorescence techniques together with TDDFT electronic calculations. To rationalize the behaviour of **INR** in water, the water-soluble sulfonated indirubin (**5SINR**) and the tri-sulfonated indigo (**3SIND**) were further investigated. For **INR** in viscous solvents (e.g. glycerol) ESPT is present. With the studied indirubin derivatives (exception made to **DMINR**), an additional pathway, to ESPT, exists involving rotation between the two indole-like moieties, with a *syn*-conformer, leading to a more efficient radiationless deactivation pathway, when compared to indigo. The mechanism of *syn*-conformer formation is found to involve a longer lifetime in the viscous solvent. This new deactivation process is not present in **IND**. ESPT, found to be enhanced in water via intermolecular water assisted proton transfer, with a kinetic isotopic effect (KIE = k_H/k_D), equal to 2 for **3SIND**, is also found present for **5SINR** with a KIE = 1.5. The common structural origin of the N–H···O═C bonds in the DNA nucleotides and the indigoid dyes (**INR** and **IND**), introduces a new perspective for the study of the molecular protective mechanisms in these molecules.

1. Introduction

Both understanding of the historical significance of traditional dyes and the development of related organic based chromophores for advanced materials applications benefits from knowledge on the nature of its stability [1–13]. Indirubin and indigo, Scheme 1, are the core representatives of a small group of bis-indole alkaloids belonging to the indigoids family [1–4,14]. The blue dye indigo is in the genesis of the dye industry [15,16], with its manufacture historically linking the Western and Muslim civilizations [3,4,17–19]. Indirubin imparts a red shade to indigo denims and reported for millennia to be the active ingredient of traditional Chinese Medicine, *Danggui Longhui Wan*, potentially used in the treatment of chronic myelocytic leukemia, despite the fact that its mechanism of action is not understood [20,21]. Inhibition of cyclin-dependent kinases, known to exercise crucial functions in regulating the cell division cycle and of glycogen synthase kinase, have been proposed as the mechanism involved in the interaction of indirubin and cancer cells [22]. Phototoxicity, presumably involving reactive oxygen species production, has also been reported for indirubin derivatives [12].

The longevity of indigo as a dye is due to its extraordinary light stability, with very low photodegradation quantum yields [6], associated to the dominance, in the deactivation of the excited state, of the dark (radiationless) internal conversion process [1–3,23]. More than 99.99% of the excited state deactivates through this channel, with negligible contributions from fluorescence [23–25] and intersystem crossing [26,27]. With more or less complex interpretations, the mechanism behind this extremely efficient process has been shown, both experimen-

* Corresponding author.
E-mail address: sseixas@ci.uc.pt (J.Sérgio Seixas de Melo).
[1] Present Addresses University of Coimbra, CQC-ISM, Department of Chemistry, Rua Larga, 3004-535 Coimbra, Portugal.

https://doi.org/10.1016/j.dyepig.2023.111116
Received 19 September 2022; Received in revised form 13 January 2023; Accepted 16 January 2023
0143-7208/

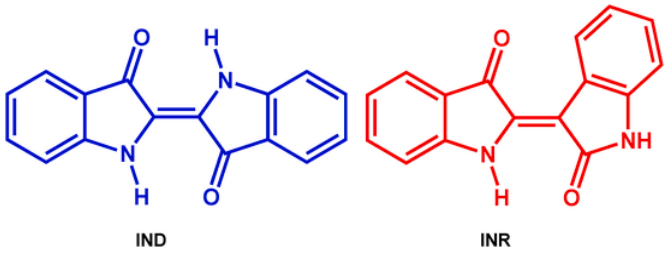

Scheme 1. Molecular structures of indigo (**IND**) and indirubin (**INR**).

tally and theoretically, to involve a single proton transfer in the excited state [1,28–33].

Excited-state proton transfer (ESPT) plays a major role in chemical and biological systems, such as photosystem II, bacteriorhodopsin, and green fluorescence protein. Indigo, indirubin, and DNA bases share a common molecular structure with N–H···O═C hydrogen bonds (Scheme 2) [1,3,4,34]. Besides linking the DNA bases in the double helix, hydrogen bonding is present in indigo and related systems, and associated to the molecular mechanism that explains its photostability [1–4,28,29]. Indeed, with indigo, the fast-excited state proton transfer minimizes access to other potential processes such as light induced degradation, consistent with a photoprotective mechanism shared with many other dyes and with the bases of DNA (see Scheme 2) [35]. The common origin of the DNA nucleotides and indigo dyes, which is also associated to its longevity on Earth, has led to coining these molecules as molecular fossils [4,34].

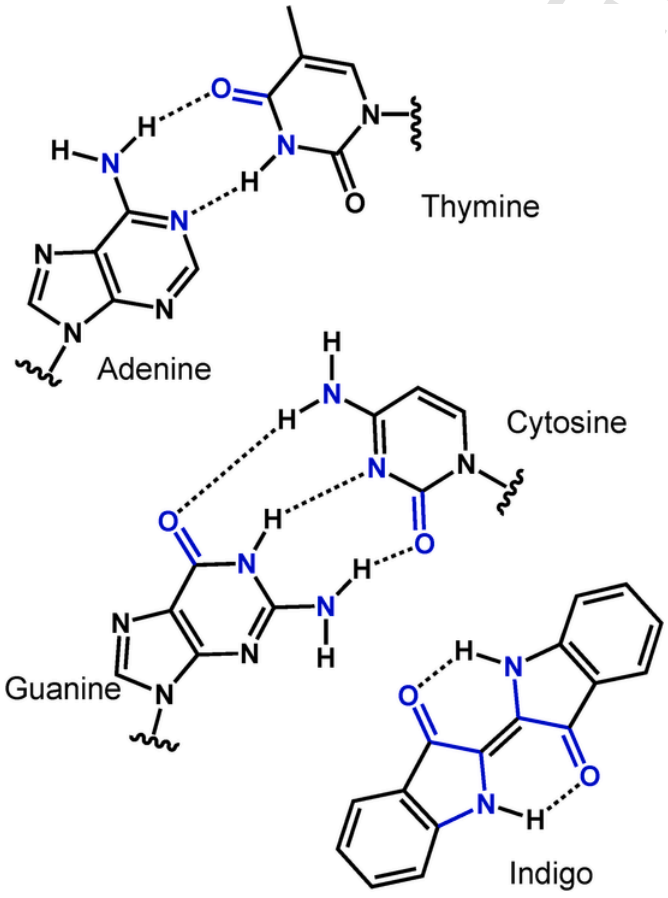

Scheme 2. Chemical structures of the DNA nucleotides adenine, guanine, cytosine and thymine together with indigo, showing the close similarity of the N–H···O═C hydrogen bonds existent in the molecules.

Indirubin is structurally constituted by half-moieties of isatin and indigo, joined by a central C═C double bond (Scheme 1). Although **INR** is an isomer of indigo, the closer proximity of the amine hydrogen present in the half-indigo and the keto oxygen in the isatin moiety, as well as the lack of hydrogen bonding interaction, between the keto oxygen in the half-indigo moiety to the amine hydrogen in the isatin piece, can dramatically change the photophysics of this molecule.

In order to fully elucidate the properties and stability of indirubin, the synthesis and a comprehensive characterization of a series of indirubin derivatives with different substituents was made aiming to rationalize its deactivation mechanisms. Furthermore, a comparison with indigo and one water soluble derivative was undertaken. From a comprehensive photophysical characterization, in different solvents, including ultrafast spectroscopic techniques, density functional theory (DFT) and time dependent DFT (TDDFT) studies, the decay mechanisms in indirubin are unveiled.

2. Experimental section

2.1. Materials and methods

The chemicals were obtained from commercial sources and used as received. Water was twice distilled and passed through a Millipore apparatus. All the solvents (spectroscopic or equivalent grade) were used without further purification. Microwave-assisted synthesis was performed using a CEM Discover S-Class single-mode microwave reactor, featuring continuous temperature, pressure and microwave power monitoring. ^{1}H NMR and ^{13}C NMR spectra were recorded on a Bruker Avance III spectrometer with operating frequencies of 400 and 101 MHz, respectively. High-resolution mass spectrometry (HRMS) was performed on a Bruker microTOF-Focus mass spectrometer equipped with an electrospray ionization time-of-flight (ESI-TOF) source.

2.2. Synthesis

Indigo and tri-sulphonated indigo were obtained from Sigma-Aldrich and used without further purification; analysis of the substitution of the tri-sulphonated indigo was studied by NMR (see Figs. SI10-SI31). The overall synthetic scheme for the synthetized compounds can be found in **Scheme SI1**. To obtain indirubin, the general procedure from Russell and Kaupp, where the acetyl indoxyl is reacted with the corresponding isatin was followed [36]. This synthetic protocol, dated from 1969, has been extensively used for obtaining different indirubin derivatives, including those reported in this paper. However, since the photophysical studies require a high level of purity, additional purification methods were needed and were added to the reported synthesis to be sure that no indigo was present, as an impurity, in the synthesized compounds. For this reason, synthetic modifications were introduced in the reported protocols. Previous synthetic reports, together with the analytical characterization, have been previously reported for indirubin [37], 5-sulphonic acid indirubin [38], *N*-methylindirubin [39] and *N,N′*-dimethylindirubin [40].

5,5′,7-trisulfonic acid indigo tripotassium salt (or 5,5′,7-Indigotrisulfonic acid tripotassium salt) (3SIND). ^{1}H NMR (400 MHz, D_2O) δ (ppm): 8.16 (s, 1H), 8.14 (s, 1H), 8.03 (s, 1H), 7.89 (d, J = 8.7 Hz, 1H), 7.12 (d, J = 8.7 Hz, 1H). **^{13}C NMR** (101 MHz, D_2O) δ (ppm): 189.2, 186.8, 153.6, 147.6, 135.7, 135.3, 134.1, 130.4, 126.4, 124.6, 122.6, 122.0, 121.5, 120.6, 118.7, 113.3. (Figs. SI10-SI14).

2.2.1 Synthesis of indirubin and substituted indirubin derivatives (the synthetic procedure was taken from Refs. [37,38]; however, some experimental modifications were carried out in order to discard, even if vestigial, indigo formation as an impurity): 50 mL of methanol were degassed during 20 min by continuously bubbling nitrogen into

the solution. Then, 3-indoxyl acetate (200 mg, 1.14 mmol), K_2CO_3 (1.9 mmol) and the corresponding isatin derivative (1.14 mmol) were added to the round bottom flask, keeping the solution under nitrogen bubbling and stirring for 45 min. The precipitate was collected by filtration and washed successively with the appropriate cold solvent to yield the desired compound as reddish solids. Although the NMR seemed correctly, traces of indigo were observed in the excitation spectrum (λ_{em} = 690 nm) by the presence of a shoulder centered at 608 nm. Therefore, purification by column chromatography was performed.

Indirubin (INR) was prepared by the above described procedure using isatin (169 mg) as reactant. The obtained precipitated was washed with cold methanol and purified by column chromatography (silica; CH_2Cl_2) to afford **(INR)** as a reddish solid (193 mg, 64%).

^{1}H NMR (400 MHz, DMSO) δ (ppm): 11.02 (s, 1H), 10.89 (s, 1H), 8.77 (d, J = 7.8 Hz, 1H), 7.65 (d, J = 7.6 Hz, 1H), 7.58 (t, J = 7.7 Hz, 1H), 7.42 (d, J = 8.0 Hz, 1H), 7.25 (t, J = 7.6 Hz, 1H), 7.02 (t, J = 7.6 Hz, 2H), 6.90 (d, J = 7.6 Hz, 1H). **^{13}C NMR** (101 MHz, DMSO) δ (ppm): 188.7, 171.0, 152.5, 141.0, 138.4, 137.1, 129.3, 124.7, 124.4, 121.5, 121.3, 119.0, 113.5, 109.6, 106.6. (Figs. SI15-SI17). **ESI-MS** (*m/z*): Calculated for $C_{16}H_{10}N_2O_2$: 262.07; Found: $[L + H]^+$ 263.08 (Fig. SI18).

5-Sulphonic acid indirubin (5SINR). Isatin-5-sulfonic acid sodium salt dihydrate was used (327 mg) for the synthesis of **(5SINR)**. The precipitated obtained was washed with cold dichloromethane and then dissolved with water. The filtrate was dried under vacuum and a reddish solid was obtained (263 mg, 79%).

^{1}H NMR (400 MHz, D_2O) δ (ppm): 8.77 (d, J = 1.7 Hz, 1H), 7.44 (dd, J_1 = 8.2 Hz, J_2 = 1.8 Hz, 1H), 7.27 (d, J = 7.5 Hz, 1H), 7.07 (t, J = 8.2 Hz, 1H), 6.67 (t, J = 7.4 Hz, 1H), 6.59 (d, J = 8.2 Hz, 1H), 6.45 (d, J = 8.0 Hz, 1H). **DEPT NMR** (101 MHz, D_2O) δ (ppm): 137.7, 126.4, 124.2, 122.0, 121.8, 112.1, 109.8 (Figs. SI19 and **SI20**). **^{1}H NMR** (400 MHz, DMSO) δ (ppm): 10.93 (s, 1H), 10.85 (s, 1H), 9.36 (d, J = 1.7 Hz, 1H), 9.03 (d, J = 7 Hz, 1H), 7.60 (dd, J_1 = 8.1 Hz, J_2 = 1.8 Hz, 1H), 7.33 (dt, J_1 = 6.4 Hz, J_2 = 1.3 Hz, 1H), 6.96 (t, J = 7.2 Hz, 1H), 6.83 (d, J = 7.8 Hz, 1H), 6.5 (d, J = 8.1 Hz, 1H). **^{13}C NMR** (101 MHz, DMSO) δ (ppm): 169.7, 169.2, 144.8, 144.4, 142.8, 134.0, 133.8, 133.2, 130.6, 129.8, 127.6, 122.2, 121.5, 121.2, 110.0, 108.7. (Figs. SI21 and **SI22**). **ESI-MS** (*m/z*): Calculated for $C_{16}H_{10}N_2O_5S$: 342.03; Found: $[L + H]^+$ 343.03 (Fig. SI23).

2.2.1. Synthesis of N and N,N' methyl indirubin

***N*-methylindirubin (MINR)** was prepared by using 1-methylisatin as reactant (185 mg). The precipitate obtained during the reaction was filtered and washed with cold methanol. Then, column chromatography was performed to purify the solid (sílica; hexane- CH_2Cl_2: 1:9) (279 mg, 71%).

^{1}H NMR (400 MHz, $CDCl_3$) δ (ppm):10.54 (s, 1H), 8.88 (d, J = 7.7 Hz, 1H), 7.73 (d, J = 7.5 Hz, 1H), 7.51 (t, J = 7.2 Hz, 1H), 7.33 (d, J = 8 Hz, 1H), 7.15 (t, J = 7.7 Hz, 1H), 7.03–6.99 (m, 2H), 7.00 (m, 2H), 6.87 (t, J = 7.3 Hz, 1H), 3.34 (s, 3H). **^{13}C NMR** (400 MHz, $CDCl_3$) δ (ppm): 188.4, 170.7, 151.7, 142.0, 139.3, 137.0, 129.2, 125.5, 125.3, 122.7, 121.6, 121.1, 120.1, 112.0, 107.9, 29.7. (Figs. SI24-**SI26**). **ESI-MS** (*m/z*): Calculated for $C_{17}H_{12}N_2O_2$: 276.08; Found: $[L + H]^+$ 277.09 (Fig. SI27).

***N,N'*-dimethylindirubin (DMINR)** The synthesis of this compound has been previously reported [40]. However, in this paper we have followed an alternative synthetic procedure described in Ref. [41], there established for the alkylation of an acridone. A mixture of **MINR** (100 mg, 0.36 mmol), K_2CO_3 (32 mg, 0.36 mmol), Al_2O_3 (140 mg, 2.17 mmol), NaOH (21 mg, 0.83 mmol) and TBAB (7.37 mg, 0.04 mmol) were placed into a 10 mL microwave tube. Then, iodomethane (0.14 mL, 3.62 mmol) was added and heated under microwave radiation (30 min, 65 °C), with high speed stirring using a CEM (Discover SP) microwave oven. The reaction mixture was cooled at room temperature and the crude was purified by column chromatography (sílica; CH_2Cl_2). A purple solid was obtained (42 mg, 38%).

^{1}H NMR (400 MHz, $CDCl_3$) δ (ppm): 8.60 (d, J = 7.8 Hz, 1H), 7.70 (d, J = 7.4 Hz, 1H), 7.57 (t, J = 7.5 Hz, 1H), 7.29 (t, J = 7.7 Hz, 1H), 7.10–7.03 (m, 3H), 6.83 (d, J = 7.8 Hz, 1H), 3.61 (s, 3H), 3.31 (s, 3H). **^{13}C NMR** (400 MHz, $CDCl_3$) δ (ppm): 188.6, 166.9, 154.9, 143.2, 142.7, 136.8, 129.5, 125.1, 124.9, 122.5, 122.4, 122.0, 121.1, 111.2, 109.4, 107.8, 77.2, 38.00, 26.37. (Figs. SI28-SI30). **ESI-MS** (*m/z*): Calculated for $C_{18}H_{14}N_2O_2$: 290.10; Found: $[L + H]^+$ 291.11 (Fig. SI31).

2.3. Photophysical measurements

Absorption spectra were recorded on a Cary 5000 UV–Vis–NIR. Fluorescence spectra were recorded in a Horiba-Jobin-Yvon Spex Fluorolog 3–2.2. Spectrophotometer and corrected for the instrumental response of the system. The fluorescence quantum yields of the compounds were determined using indigo as standard (φ_F = 0.0023 in DMF) and indirubin (φ_F = 0.0003 in DMF) [25]. Overall the error associated to the measured φ_F values varied from 1% to ca. 9%.

Femtosecond Transient Absorption Spectroscopy (fs-TA) experiments were performed with a Helios spectrometer (Ultrafast Systems) with an instrumental response function of ~250 fs. The instrumental response function of the system was assumed to be equal to that of the pump–probe cross correlation determined from the measurement of the instantaneous stimulated Raman signal from the pure solvent (in a 2 mm cuvette). To avoid photodegradation, the solutions were stirred during the experiments or in movement using a motorized translating sample holder. The spectral chirp of the data was corrected using the Surface Xplorer PRO program from Ultrafast Systems.

Fluorescence decays were measured using a broad band femtosecond fluorescence up conversion, fs-UC, Halcyone Fire spectrometer from Ultrafast Systems (thermoelectrically cooled, −40 °C, CCD detectors with spectral range from the UV, ~270–400 nm, Vis, 400–800 nm, to the NIR, ~800–1600 nm), pumped by a 1 kHz Spectra Physics Solstice-Ace laser (7 W, 800 nm and 120 fs IRF) coupled to an TOPAS Prime optical parametric amplifier (OPA) with 235–2600 nm automatic tuning range. The fs-UC spectrometer comprises a delay stage and Ultrafast Systems OPA to generate the gate pulse at 800 nm or 1300 nm with a time resolution of 100 fs and time window for acquisition up to 8 ns. The time-resolved fluorescence spectra was obtained with excitation at 450 nm and 530 nm by sum frequency of the fluorescence emission with an 800 nm gate pulse in a BBO crystal. Global and Target analysis of the data was performed using principal component Analysis via single value decomposition (SVD) implemented in the Surface Xplorer Pro program package from Ultrafast Systems and Glotaran [42].

2.4. Quantum electronic calculations

All theoretical calculations were of the DFT type, carried out using GAMESS-US [43]version R3, using as functional the implemented version of LC-BPBE (ω = 0.20 au^{-1}). In TDDFT calculations of FC (Franck-Condon) excitations the dielectric constant of the solvent was split into a "bulk" component and a fast component, which is essentially the square of the refractive index. In "adiabatic" conditions only the static dielectric constant is used. A 6-31G** basis set was used in either DFT or TDDFT calculations.

The results obtained with the LC-BPBE(20) functional are essentially unscaled raw data from calculations; for the $S_0 \rightarrow S_n$ transitions, a small correction, which result in the subtraction of 0.05 eV, to account for the difference between zero point and the first vibronic level, was considered. For the resulting optimized geometries time dependent DFT calculations (using the same functional and basis set as those in the previously calculations) were performed to predict the vertical electronic ex-

citation energies. Molecular orbital contours were plotted using ChemCraft 1.7 program. Frequency analysis for each compound were also computed and did not yield any imaginary frequencies, indicating that the structure of each molecule corresponds to at least a local minimum on the potential energy surface.

Probing of the potential energy surface to locate the conical intersection (CI) was based on the anchor points defined by the enol and *syn*-rotamer enol S_1 optimized structures connected to the apex of the isomerization barrier by an IRC (internal reaction coordinate). By using Hessians along this IRC path, we identified possible reactive normal modes, parallel to the IRC, that could correspond to the branching space of the Conical Intersection (CI) and, along them, minimized $\Delta E = E(S_1)\text{-}E(S_0)$ until a predefined threshold of 0.05 eV (or less) was observed [29,44,45].

3. Results and discussion

Structures and acronyms of the core structures of indigo (**IND**) and indirubin (**INR**), together with the mono-*N*-methyl (**MINR**) and *N,N′*-dimethyl (**DMINR**) indirubin derivatives and the water-soluble derivative 5-sulfonic acid indirubin (**5SINR**), synthesized in this work, and the water-soluble indigo 5,5′,7-trisulfonic acid indigo (**3SIND**), are depicted in Schemes 1 and 3. In the following sections, we will address the rationalization of the nature of the different absorption (and colour) in indirubin (red) in comparison with indigo (blue) and of the high photostability in **INR** (and derivatives) at the light of the excited state decay processes.

3.1. Absorption and steady state fluorescence spectral data

Absorption and fluorescence spectra of indirubin (**INR**) together with different indirubin (**MINR**, **DMINR**, **5SINR** and **3SIND**) derivatives were obtained in different organic solvents with different dielectric constant (polarity) and viscosity values at room temperature (T = 293 K), Fig. 1. Indigo (**IND**) is included for comparison [28]. From Fig. 1 pertinent observations are that (**i**) the absorption and emission of **INR** are blue-shifted relative to **IND**; the (**ii**) absorption (and fluorescence) spectra of **INR** red-shifts upon increase of the media polarity, from 531 nm in Dx to 546 nm in DMF (Table 1) and that (**iii**), also in comparison with **IND**, it is worth noticing the much larger Stokes Shift value (Δ_{SS}) observed, in particular in highly viscous solvents such as glycerol, with values of 1080 cm^{-1} for **IND** in DMF and 3455 cm^{-1} for **INR**, see Table 1.

From all of the above, which will be further consubstantiated in section 3.2, the H-chromophore (donor-acceptor, N–H and C═O groups in a H-type configuration) [3,46,47] of **IND** is also found present in **INR**. Furthermore, compared with **IND** and besides the blueshift of the bands, the Stokes' shift values for **INR** and its derivatives (**MINR**, **DMINR** and **5SINR**) more than tripled, with the highest Δ_{SS} value (four times higher) for **5SINR** in methanol and the very poorly fluorescent **DMINR** in dioxane. Moreover, the spectral characteristics of **IND** are found identical to its water-soluble derivative, **3SIND**, and the same is valid for **INR** and **5SINR**. Table 1 summarizes the spectral data for indirubin derivatives and indigo in different solvents with different polarity and viscosity.

A more careful observation of Fig. 1 shows that the full width at half maximum (FWHM) of the emission band of **INR** gives a direct evidence that in glycerol (with FWHM = 3481 cm^{-1}) the emission spectra likely involves convolution of more than one contributing species - the keto and enol forms- with a higher contribution of the more emissive enol when compared with other non-viscous solvents such as dioxane (FWHM = 3120 cm^{-1}).

Mono- and di-methylation of the amine group in **INR** introduces relevant electronic spectral changes, consequence of the different contributions to the ground and excited state potential energy curves. Analysis of the spectra shows that methyl substitution (**MINR**) keeps the wavelength maxima (absorption and emission) approximately identical to that of **INR** and, consequently, of the Δ_{SS} value, whereas with *N,N′*-dimethyl substitution (**DMINR**), a larger red-shift of the absorption and emission maxima is now observed (Fig. 1). These evidences allow us to conclude that the deactivation mechanism is different in **MINR** and **DMINR**. The presence of different conformational structures (for different indirubin derivatives) in the excited state will be further considered from the time-resolved data summarized in Table 3 and rationalized from DFT and TDDFT calculations.

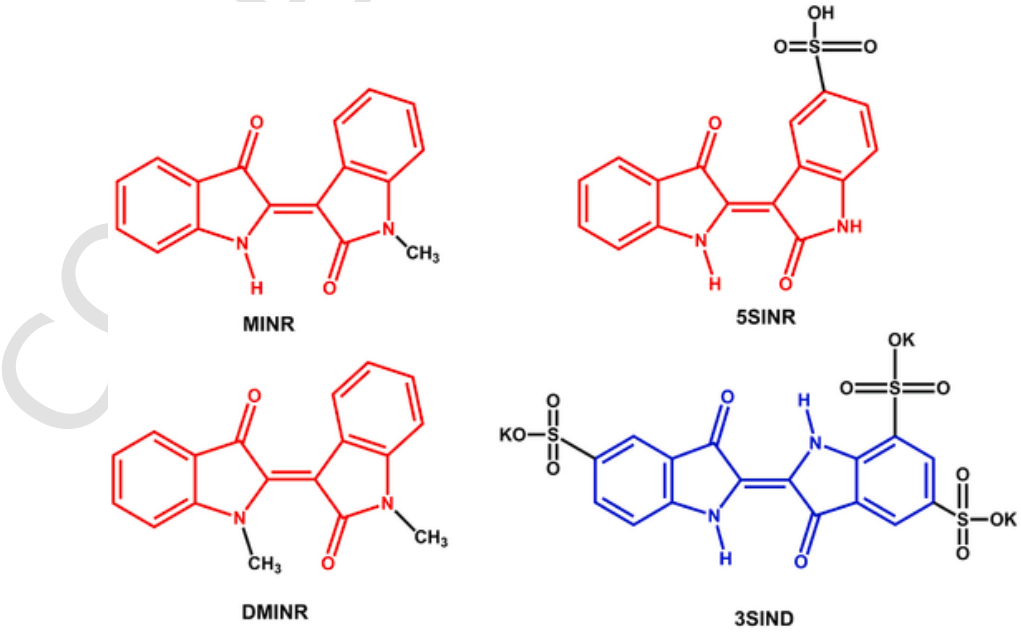

Scheme 3. Chemical structures and acronyms of the sulfonated derivative *N′*-methyl indirubin (**MINR**), indirubin 5-sulfonic acid (**5SINR**), *N,N′*-dimethyl indirubin (**DMINR**) and indigo 5,5′,7-trisulfonic acid (**3SIND**).

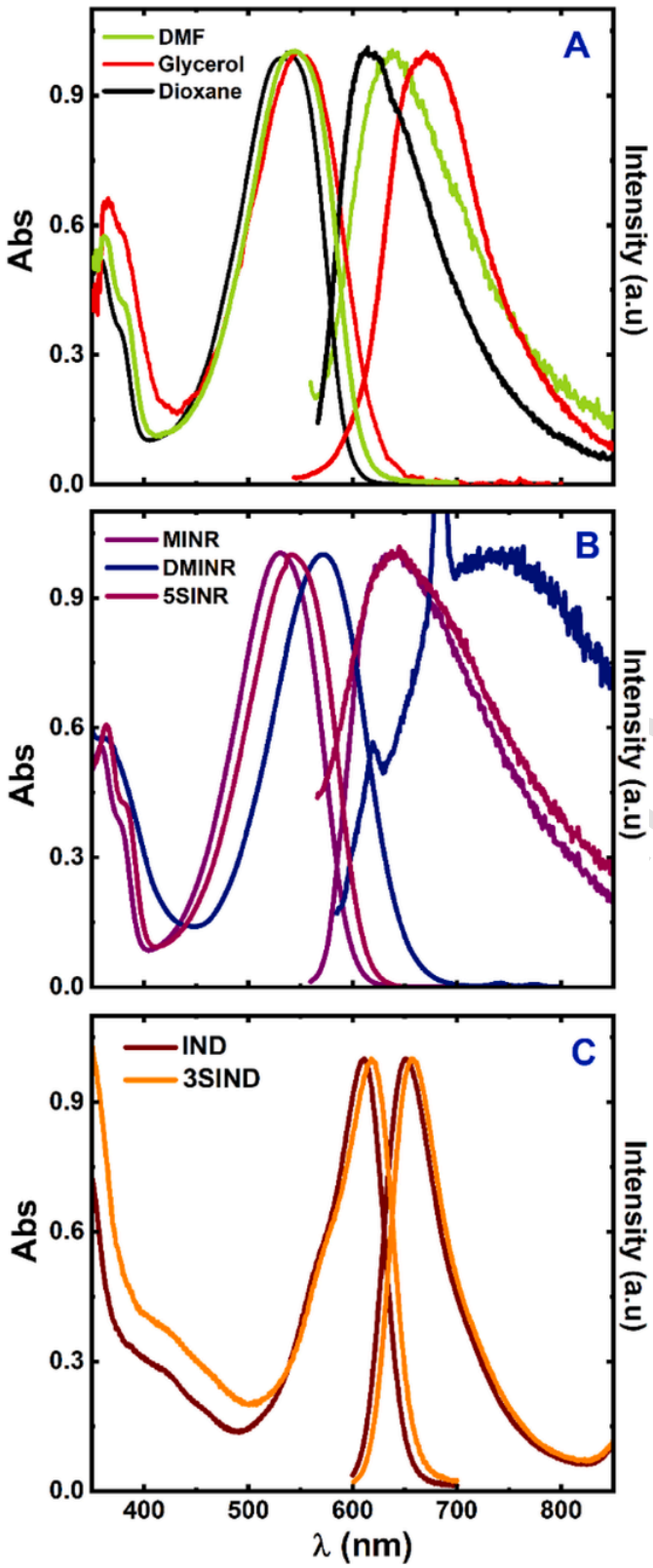

Fig. 1. Normalized absorption and fluorescence spectra of (**A**) **INR** in different solvents (as indicated in the inset caption); (**B**) **MINR** and **DMINR** in DMF and **5SINR** in dioxane and (**C**) **IND** and **3SIND** in DMF at T = 293 K.

Table 1
Spectroscopic properties, including wavelength maxima for absorption (λ_{max}^{abs}), fluorescence (λ_{max}^{em}) and Stokes shift (Δ_{SS}) for **INR**, **MINR**, **DMINR**, **5SNR**, **IND** and **3SIND** in different organic solvents at T = 293 K. For indigo the same parameters are also presented (in DMF) for comparison.

Cmpd	Solvent	λ_{max}^{abs} (nm)	λ_{max}^{em} (nm)	Δ_{SS} (cm^{-1})
INR	Glycerol	548	676	3460
	DMF	546	638	2640
	Methanol	537	633	2820
	2MeTHF	531	635	3080
MINR	DMF	547	648	2850
	2MeTHF	532	633	3000
	Dioxane	531	647	3380
DMINR	DMF	583	750	3820
	2MeTHF	567	620	1510
	Dioxane	573	744	4010
5SINR	Water	536	639	3010
	DMF	542	645	2950
	Methanol	545	694	3940
IND[a)]	DMF	610	653	1080
3SIND	Water	598	672	1840
	Glycerol	607	646	1000
	DMF	618	656	940

[a] Data from ref. [25].

Table 3
Comparison of the fluorescence decay times, τ_i., obtained from femtosecond Transient Absorption (fs-TA) and femtosecond fluorescence UpConversion (fs-UC) measurements for **INR**, **MINR**, **DMINR**, **5SINR** and **3SIND** at T = 293 K in solvents of different polarity and viscosity. The values result from global and target analysis of the data. Some examples of raw data and fs-TA target analysis of INR in dioxane (**Fig SI3**), in glycerol (Fig. SI4) and of fs-UC (Fig. SI5) and for fs-UC for MINR (Fig. SI6) are given in SI.

Comp.	Solvent	fs-TA			fs-UC		
		τ_1 (ps)	τ_2 (ps)	τ_3 (ps)	τ_1 (ps)	τ_2 (ps)	τ_3 (ps)
INR	**Dioxane**	–	–	38	–	3	37
	2MeTHF	–	–	32	–	3	29
	MeOH	–	2	12	–	–	–
	DMF	–	1.8*	14	–	1	8
	Glycerol	–	16	50	–	–	–
MINR	**Dioxane**	–	2*	14	–	1.4	8.4
	2MeTHF	–	2*	14	–	1.4	8
	DMF	–	1*	8	–	0.8	3
DMINR	**Dioxane**	0.9	6	–	–	–	–
	2MeTHF	0.7	6	–	0.3	1.6	–
	DMF	0.4	4	–	0.2	1.3	–
5SINR	**MeOH**	–	3.03*	12.6	–	–	–
	MeOD	–	3.85*	14	–	–	–
	H_2O	–	–	2.49	–	–	–
	D_2O	–	–	3.27	–	–	–
	Glycerol	–	15	48	–	–	–
3SIND	**DMF**	–	2	126	–	–	–
	H_2O	–	0.72	4.62	–	0.313	2.02
	H_2O: D_2O (1:1)	–	–	–	–	0.646	4.09
	Glycerol	–	88	539	–	–	–

* The decay component is associated to a negative amplitude (rise-time).

3.2. The H-chromophore and the colour of indirubin

Fig. 2 maps the orbital contours of the highest occupied molecular orbital (HOMO) and lowest unoccupied molecular orbital (LUMO) for the indigo (**IND**) and indirubin (**INR**). The transition in **INR** retains the nature of the donor and acceptor groups in **IND** (the H-chromophore), but the comparison between the HOMO and LUMO of the two compounds shows that the former is, with **INR**, energetically lower. Indeed, with **INR** the HOMO has a more extended bond delocalization (connecting the two indole-like molecules through the

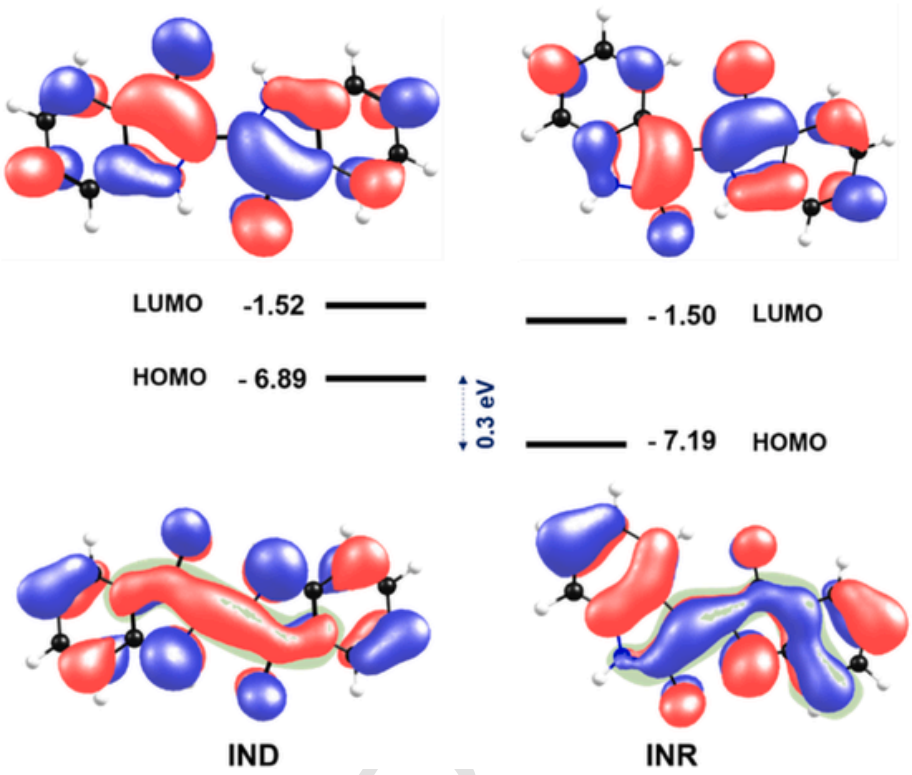

Fig. 2. Orbital contours of the HOMO and LUMO for the indigo (**IND**) and indirubin (**INR**) in DMF.

central carbon-carbon bond) than that in **IND**. As a consequence of this extended bond delocalization, in **INR**, it mainly contribute to a stabilization of the HOMO - relative to **IND**-, and since the LUMO is almost unaffected, in the two compounds, it leads to the observed blue-shift of the predicted transition (see **Table SI1**) and of the experimental band spectra (Fig. 1). However, the most interesting feature in **INR** is found in the hydrogen bond N–H···O═C distance with a value of 186 pm in S_0 (for **IND** the same bond distance is 224 pm) whereas in S_1 the value is 170 pm (199 pm for **IND**), see Fig. SI1. These different values show that both in S_0 and S_1, the hydrogen N–H ···O═C bond distance is smaller in **INR** which indicates that intramolecular excited state proton transfer (ESPIT) will be favoured relative to **IND**.

3.3. The photophysics unveiling the photostability of indirubin

3.3.1. Fluorescence quantum yields

From the fluorescence quantum yield (φ_F) values, depicted in Table 2, three main observations can be highlighted. First, **(i) INR** and all its derivatives display fluorescence quantum yields that are, at least, one order of magnitude lower than **IND** and **3SIND**. Second (**ii**), **INR** in glycerol is seen to an exception, with the φ_F value doubling that of **IND**. As will be discussed at the light of the time-resolved measurements, this is related to a strong decrease of the radiationless decay in **INR** due to the high viscosity of glycerol. Since ESIPT is still a viable excited state deactivation route, the decrease of the non-radiative process should be related to a viscosity barrier that slows down the process of rotation around the central carbon-carbon bond. This hypothesis was further checked with TDDFT calculations. Finally (**iii**) comparison of the φ_F values for **MINR**, **DMINR** and **5SINR** shows that these displays, in all solvents, values that are smaller than those of **INR**, thus indicating that the radiationless deactivation pathway is more efficient with the former derivatives.

Table 2
Photophysical properties including fluorescence quantum yields (φ_F), lifetimes (τ_F) and rate constants (k_F, k_{NR}) for **INR**, **MINR**, **DMINR**, **5SINR**, **IND** and **3SIND** in solvents of different polarity and viscosity at T = 293 K.

Comp.	Solvent	φ_F	τ_F (ps)[b]	k_F (s^{-1}) x 10^7	k_{NR} (s^{-1}) x 10^{11}	k_{NR}/k_F
INR	Glycerol	0.0043	50	8.60	0.199	232
	DMF	0.0003	14	2.14	0.714	3332
	Methanol	0.0006	12	5.00	0.833	1666
	2MeTHF	0.0002	32	0.625	0.312	4999
MINR	DMF	0.000086	8	1.08	1.25	11627
	2MeTHF	0.00026	14	1.86	0.714	3845
	Dioxane	0.00022	14	1.57	0.714	4544
DMINR	2MeTHF	0.000074	6	1.23	1.67	13513
	Dioxane	0.000063	6	1.05	1.67	15872
5SINR	Water	0.000017	2.49	0.683	4.02	58823
	Methanol	0.0002	12.64	1.58	0.791	4999
IND[a]	DMF	0.0023	135	1.70	0.0739	434
3SIND	Water	0.0001	2.015	4.96	4.96	9999
	Glycerol	0.0022	539	0.408	0.0185	454
	DMF	0.0024	126	1.90	0.0792	416

[a] Data taken from ref. [25].
[b] The decays are single or bi-exponentials; when bi-exponentials the value in the table is the longer (major) decay component.

3.3.2. Rates of excited state deactivation pathways

Absence of transient absorption in ns-ms time-scales additionally indicates the absence of triplet state formation and, as with **IND**, the internal conversion $S_1 \sim\sim > S_0$ deactivation dominates the radiationless decay [27]. Indeed, as with **IND**, the absence of an efficient $S_1 \sim\sim > T_1$ deactivation channel and the very low φ_F value shows that the $S_1 \sim\sim > S_0$ internal conversion constitutes the major deactivation channel in **INR**. Moreover, from the time-resolved data (Tables 2 and 3) the longer component, τ_3, is always the major decay component, with the shorter decay (τ_2) component either associated to a rising component (negative preexponential) or to a minor contribution (although with a positive preexponential factor). Therefore, the τ_F value

can be associated to the τ_3 decay component. Nevertheless, avoiding using average lifetimes, since they do not translate any physical meaning of the system, even if the other (τ_2) decay component was consider for the k_F and k_{NR} determination, and since it has the same order of magnitude of τ_3, it would lead to similar k_{NR} values, and therefore to identical k_{NR}/k_F ratio, and to the fact that the radiationless $S_1 \sim\sim > S_0$ channel dominates the photophysics of **INR**. Therefore, from the φ_F and the longer decay time component, τ_3, of the bi-exponential fluorescence decays (see Tables 2 and 3, respectively), the radiative (k_F) and radiationless (k_{NR}) rate constants were obtained, in Table 2, showing that the radiationless processes largely dominates the deactivation of the excited state.

However, further comparison between **IND** and **3SIND** shows that the molecular mechanism behind this efficient deactivation should be different in **INR**. In particular this becomes evident from the ratio of the radiationless and radiative rate constants (Table 2), k_{NR}/k_F, found one to two orders of magnitude higher in **INR** (and derivatives) than in **IND**. The exception is, once more, **INR** in glycerol. With **DMINR**, where ESIPT is blocked, an increase on the radiative deactivation channel would be potentially observed. However, contrasting with this prediction, the opposite behaviour is observed with a decrease of φ_F (relative to **INR**) by a factor of three in 2MeTHF.

In view of the very poorly fluorescence quantum yields of these systems, the excited state deactivation, including the type and number of species and mechanisms, can only be properly addressed with the study of its transient spectral characteristics. Femtosecond transient difference absorption (fs-TA) and femtosecond transient up conversion (fs-UC) experiments, allow both a kinetic and band spectral analysis.

3.4. Molecular deactivation mechanisms from time-resolved experiments: fs-TA and fs-UC

Time-resolved spectra and kinetics were obtained with time-resolved femtosecond (either from fs-TA and/or fs-UC) techniques. fs-TA experiments were recorded in the 440–800 nm range, in various aerated solvents, with excitation at 530 nm, and at T = 293 K. Fig. 3 shows the fs-TA spectrum for **INR** in dioxane, dominated by a positive broad transient absorption band in the 545–655 nm range (with maxima at ~ 585 nm) attributed to the excited singlet state absorption (ESA), complemented by a negative band at longer wavelengths (655–720 nm), due to stimulated emission (SE). Similar transient difference absorption bands were found for **INR** in the other investigated solvents. Table 3 summarizes the time-resolved femtosecond data obtained for the indirubin derivatives (**INR, MINR, DMINR** and **5SINR**) and the water-soluble indigo, **3SIND**. Global analysis of the time-resolved data conduces to best fit results with a bi-exponential decay law for the majority of the indirubin derivatives and also for **3SIND**.

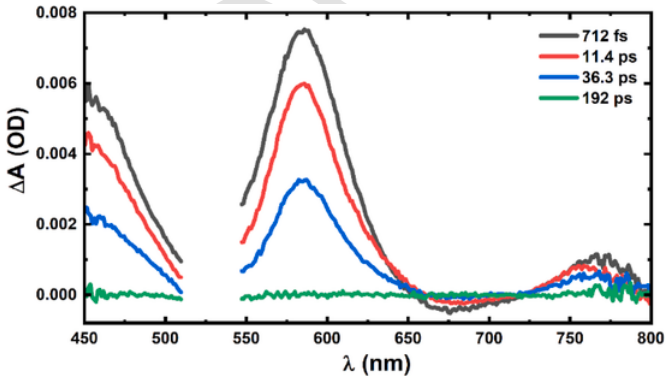

Fig. 3. Time-resolved transient absorption data for **INR** in dioxane obtained with λ_{exc} = 530 nm at T = 293 K. The 510–545 nm spectral range is not shown because it is dominated by the scattered pump beam (530 nm).

The exception is **5SINR** where single-exponential decay fittings are observed in water and deuterated water.

From previous studies, formation of *keto* and *enol* forms has been established for indigo (**IND**) and the water soluble indigo carmine (**InC**) [8,23,24,28,31,33]. Fleming et al. showed that, in protic solvents, intermolecular H-bonds in **InC** enables ESPT generating an unstable intermediate (*enol* form) that immediately reverts back to the ground state through a CI [33].

In the case of the two other decay times, these are, by paralleling with **IND** [2,3,23,24,28,48], associated to two excited kinetic species, and in this case to the *keto* and *enol* species of **INR**. From Table 3 it can be concluded that the decay components (τ_2 and τ_3), obtained from different time-resolved measurements, are likely to be associated with the presence of two excited species. This happens for almost all the studied indirubin derivatives with the exception of **DMINR** where ESPT is blocked.

Indeed, as found for **IND**, a two-state kinetic scheme in the excited state is consistent with a *keto*-excited form giving rise to the *enol* form of **INR** by fast single excited state proton transfer (sESPT) in different solvents, with short (~1–16 ps associated to the decay of the *keto* species) and long (~2–50 ps assigned to the *enol* species) decay components [28]; the range of the decay time values shows that the solvent could have a determinant role in this process.

3.5. Influence of the N- and N,N′- alkylation in indirubin

Fig. 4 depicts the fs-TA spectra for **INR**, **MINR** and **DMINR** in 2MeTHF. Analysing the fs-TA spectral features, it can be seen that **MINR** displays very similar (when compared to **INR**) ESA bands, with peaks at 588 nm and 760 nm; on the other hand, **DMINR** presents a red shift and broad ESA band centered at ca. 645 nm. However, the compounds show different kinetics (Table 3). The bi-exponential decay for **INR** and **MINR** in 2MeTHF shows that the instantaneously formed *keto* species decays with 3 ps for **INR** and 1.4 ps for **MINR**, giving rise to the *enol* species, which further decays with 29 ps (**INR**) and with 8 ps (**MINR**), to the ground state, see Table 3, Fig. 5 and Scheme 4. This indicates that the ESIPT process is faster in **MINR**. Fig. SI2 depicts the fs-UC decays of these compounds in 2MeTHF. The absence of data in glycerol for **MINR** and **DMINR** in Table 3 is due to its very poor solubility in this solvent. The fast decay time component in Table 3 (τ_1), with values from 0.2 to 0.9 ps, is in

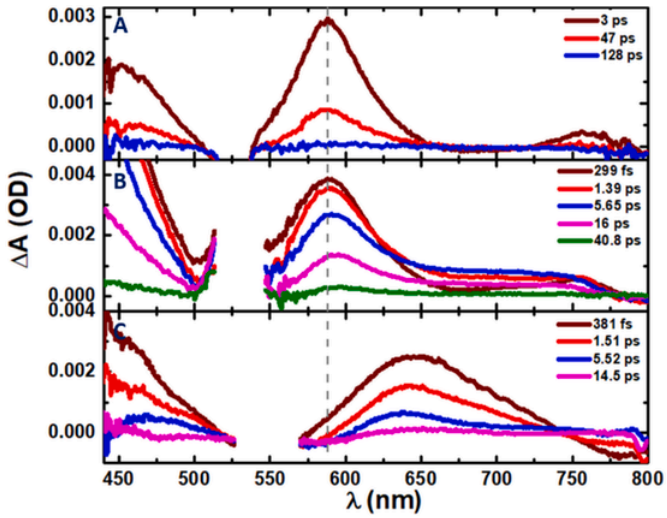

Fig. 4. fs-TA spectra for (**A**) **INR**, (**B**) **MINR** and (**C**) **DMINR** in 2MeTHF with excitation at 530 nm at T = 293 K. The vertical dashed line is just meant to be a guideline to the eye, showing the spectral shift of the ESA band for each compound.

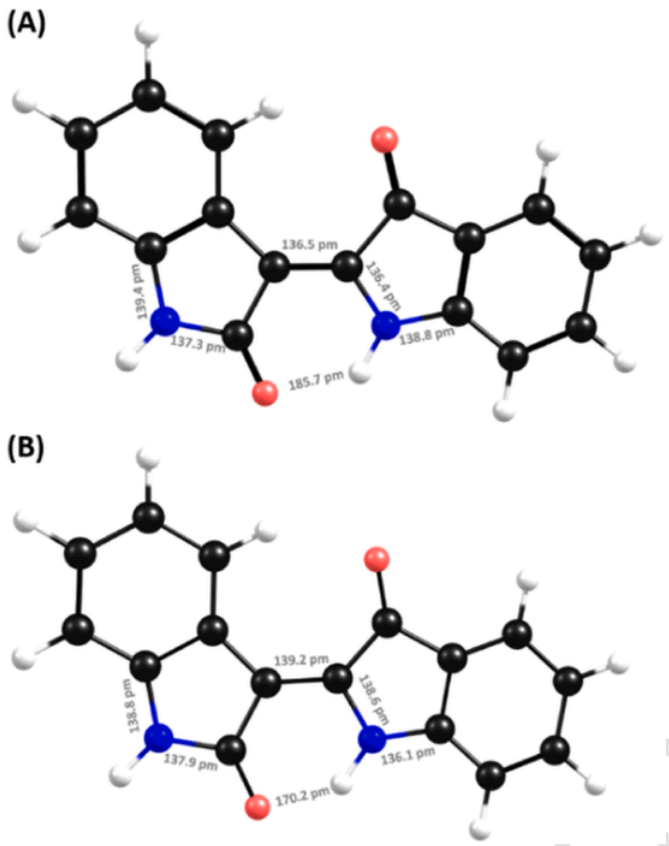

Fig. 5. Optimized structures in the S_0 (**A**) and S_1 (**B**) electronic states in DMF. The bond distance between the oxygen in C═O and the hydrogen in N–H decreases from 185.7 pm. in S_0 to 170.2 pm. in S_1, thus facilitating *enol* formation.

agreement with either solvation dynamics (the decay times reported in these solvents are found from 0.74 to 3 ps but for the C153 dye) or -since excitation was not performed in the 0−0 absorption transition band- connected to a vibrational relaxation process resulting from a hot vibrational state [49]. In any of these two situations, the fast decay time component is not directly linked to the fundamentals of the decay kinetics of the different studied compounds and can be therefore discarded from the kinetic analysis of the system [28].

It is well-known that the contribution of the *enol* species largely depends on the polarity of the solvent [28–30]. In particular, the imine-enol tautomer is favoured in polar solvents, both in the ground and/or excited state, making it easier to produce the tautomeric form.

The importance of the imine forms, Fig. 5A, in contributing to the ground-state S_0 structure, or in the corresponding first singlet excited state S_1, Fig. 5B, can be seen by comparing the C–N bond distances which are shorter when a double bond character from a specific resonant structure exists. As will be shown below the preference for the *enol* species in the excited state will have a major consequence in viscous solvents (in this case, glycerol). DFT and TDDFT calculations show that an alternative deactivation pathway must be considered. The S_1 Potential Energy Surface (PES) was probed in order to identify the non-radiative deactivation channels, in particular to characterize the location of the CI, please see **Figures SI7-SI9**.

The global picture of the decay mechanisms, both in non-polar and polar solvents, in **INR** and **MINR**, can be detailed from analysis of the TDDFT quantum electronic calculations and fs-TA data, and summarized as follows (Scheme 4 can be used as a guideline): upon excitation of (**1**) **INR** and **MINR**, they decay (with <1 ps) to a relaxed Franck-Condon (FC) state of the rapidly formed *keto* tautomer (**2**) which is followed by an activated ESIPT (**3**) – imine-enol tautomer – leading to the *enol* form (**5**), predicted to have a higher contribution in S_1. From TDDFT quantum electronic calculations, the deactivation process of **INR** and **MINR** involves, additionally to ESPT, rotation around the central C–C bond (**4**). This rotation, around -to what is now-a single bond in S_1, generates the *E*-isomer (or *syn*-conformer), which transfers the proton to the keto oxygen of the half-indigo moiety. A CI is available for this structure thus providing a very efficient non-radiative deactivation channel to the ground state (see **Figures SI7** and **SI8**) [29,30]. This

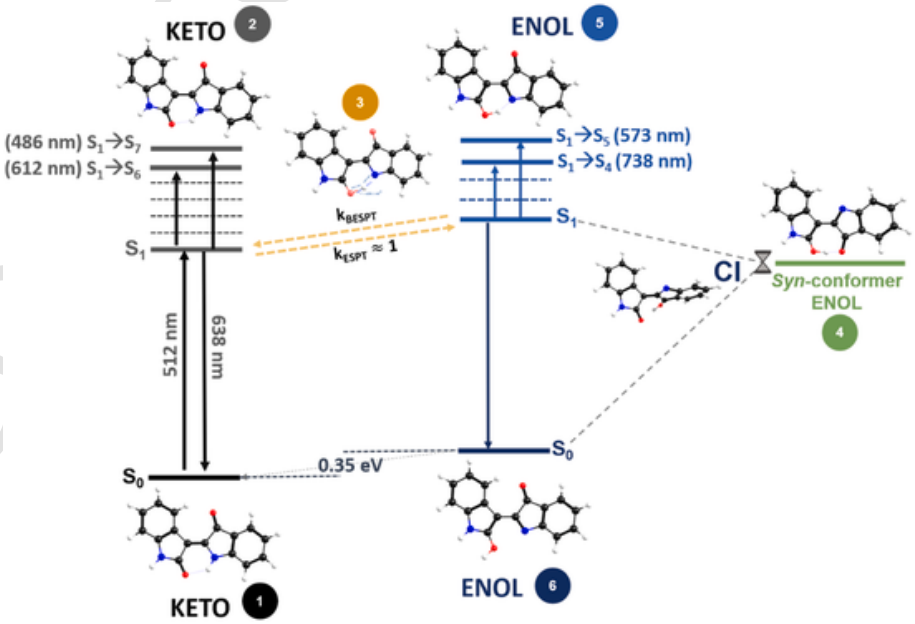

Scheme 4. Schematic diagram for the evolution of **INR**, in DMF, in the S_1 PES. The experimental transitions (from fs-TA data) are given in brackets with the corresponding transient ($S_1 \rightarrow S_n$) transitions predicted from TDDFT electronic quantum calculations. The numbering of the structures is meant to help and guide the discussion (see text); for a complete energetic diagram please see Fig. SI7 where the potential energy surface (PES) as a function of rotation around the (O═C)–C–C-(N–H) dihedral angle and occurring after proton transfer is given for INR.

process is found to exist in all solvents; however, due to the high viscosity value for glycerol, the process involving rotation around the C–C bond, leading to the formation of the *syn*-conformer and, subsequently, to the formation of the *enol*, is slow down, which is mirrored by the long decay time values associated to these species in this solvent (Table 3). If the ESPT is not present (absence of proton transfer), the rotation around the C═C bond cannot occur, due to the fact that the H-bond (between the N–H and C═O groups) is very strong, meaning that breaking this H-bond, by rotation around the central C–C bond, is energetically unfavourable thus preventing *trans*-cis photoisomerization. This has been previously evidenced with **IND** [28–30]. From Scheme 4 the transients, resulting from the $S_1 \rightarrow S_n$ transitions, obtained from the fs-TA spectral data, Figs. 3 and 4, are used to be compared with the corresponding transient transitions predicted from TDDFT electronic quantum calculations.

With **DMINR** the possibility of tautomerization is precluded and, as a consequence, rotation around the central carbon-carbon bond is now present both in the ground and excited state and, in this last case, acting as a very efficient deactivation mechanism. Absence of solvent effect in the deactivation processes is also characteristic of **DMINR**. Scheme 5 depicts the optimized structures of **DMINR** in the S_0 and S_1 states. There is a clear increase in the (O═C)–C═C-(N–CH_3) dihedral angle involving from S_0 (18°) to S_1 (36°). Linking these two states is a very distorted structure between the two half moieties linked by the central bond (almost totally perpendicular) which, geometrically, places it closer to the CI (see **Figure SI9**). Considering that the (radiationless) deactivation depends on the rate and amplitude of the torsional rotation, very fast decay times are expected when comparing **DMINR** with **MINR** and **INR**, with slower values.

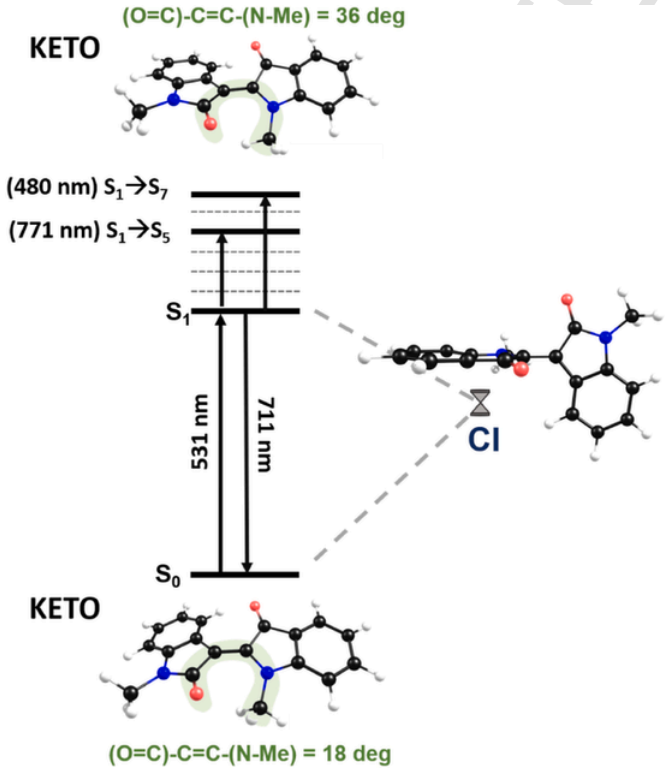

Scheme 5. Schematic diagram for the evolution of **DMINR**, in DMF, in the S_1 PES. DMINR structure in the S_0 and S_1 with the CI for the rotation around the central C═C bond. In brackets the experimental transitions (from fs-TA data) and the corresponding transient ($S_1 \rightarrow S_n$) transitions predicted from TDDFT electronic quantum calculations. The dihedral angle of 36° is indicated in green both for the S_0 and S_1 states.

3.6. Kinetic isotopic effect with the water-soluble derivatives of indigo (3SIND) and indirubin (5SINR)

Introduction of the water-soluble derivatives of indigo (**3SIND**) and indirubin (**5SINR**) in this study allows the possibility to elucidate the dynamics of **INR**, in particular competition between intra- and intermolecular ESPT. Moreover, it is worth noting the very close similarity of the values for the decay of the *keto* and *enol* forms of **IND** and **3SIND**, see Table 3. Fig. 6 depicts the fs-TA spectra for **INR** (in aprotic solvents) and for **5SINR** and **3SIND** (in water).

With **INR** two ESA bands are observed at ~580–600 nm and 775 nm, which disappear after 38 ps. For **5SINR** the fs-TA spectra in water shows an ESA band that disappears after 5 ps. In agreement with previous studies, water is found to introduce a fast and efficient radiationless deactivation channel of the excited state through water assisted intermolecular proton transfer [33,50,51].

Both the τ_2 and τ_3 values in water for **3SIND** are found very fast in particular when compared to the values found with the other compounds (Table 3). Moreover, the 0.72 ps and 4.62 ps day time values are found similar to those reported by Fleming et al. [33] for **InC** where, in comparison with a longer value of 130 ps in DMSO, the values in D_2O were found <6 ps and attributed to a solvent assisted, via intermolecular H-bonds, that facilitates ESPT. Recent studies have raised the possibility that the process may be dimer assisted making it partially intermolecular in nature [1,29,30,52]. In the case of **INR**, crystal data suggests this to be also possible [37].

Moreover, the kinetic isotopic effect (KIE) for the ESPT reaction could also be observed for **3SIND**. Data in Table 3 shows the presence of the KIE on the proton transfer reaction of **3SIND**. Indeed, from the comparison of the rate constant values (reciprocal of the decay time values) in Table 3, it can be observed that in water and water: deuterated water (1:1) the k_H/k_D is found to be ~2. For **InC** this value was found to be closed to 1.5 [53]. For **5SINR** and due to the low fluorescence quantum

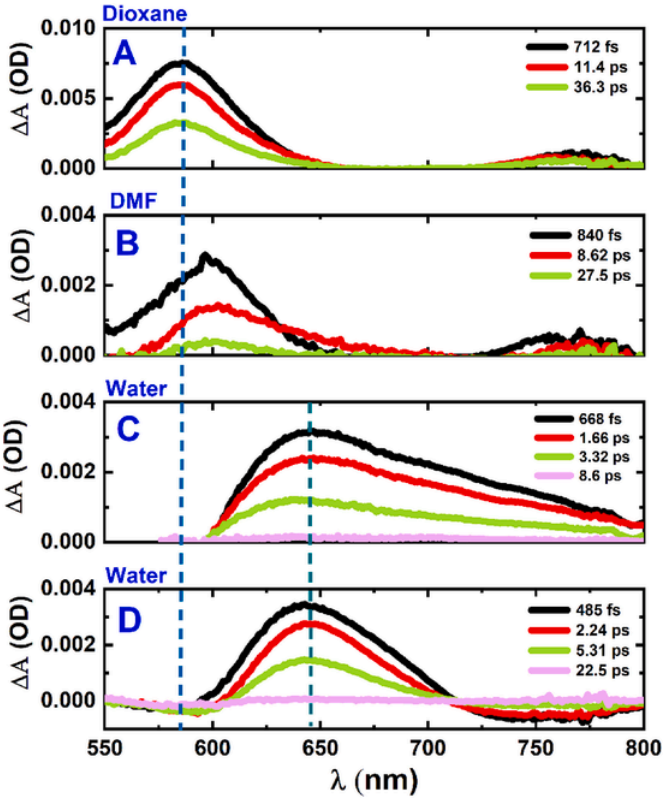

Fig. 6. fs-TA spectra for **INR** in (**A**) Dioxane and (**B**) DMF; and for (**C**) **5SINR** and (**D**) **3SIND** in water obtained with excitation at 530 nm.

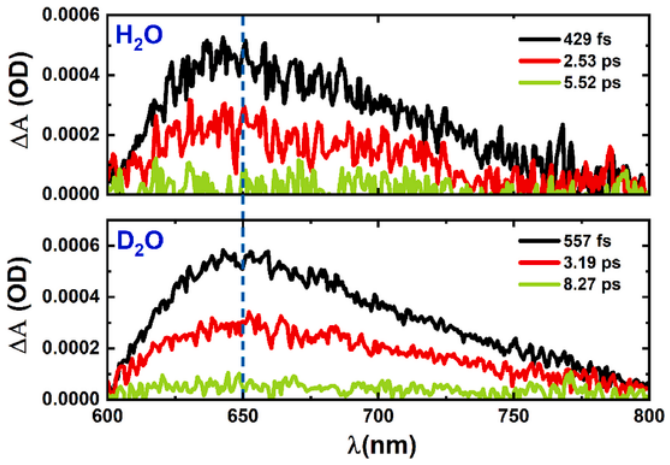

Fig. 7. fs-TA ESA bands for **5SINR** in water (top) and in deuterated water (bottom), acquired at room temperature obtained with excitation at 530 nm.

yield only fs-TA measurements could be performed, Fig. 7. Contrasting with the fs-TA spectra of **INR**, for **5SINR,** in water, a single broad band centered at ~650 nm is observed both in D_2O and H_2O, disappearing in less than 8 ps. Global and target analysis results collected in Table 3, indicate that the KIE is observed with a resulting value of 1.5, clearly demonstrating, once more, the involvement of a proton transfer in the excited state deactivation processes of these molecules.

4. Conclusion

The highly efficient dark deactivation process in **IND**, known to involve a single excited state proton transfer is also present in indirubin and linked to its high photostability. By combining steady-state and time-resolved fluorescence with fs-TA and TDDF calculations, the excited state deactivation mechanisms in **INR** could be unveiled. It was shown that the radiationless process in **INR** involves formation of a *syn*-rotamer, making this a more efficient process than with indigo. In glycerol formation of the *syn*-rotamer is hampered by solvent's viscosity, which leads to a more efficient radiative decay channel mirrored by the increase in the φ_F (and the radiative rate constant) by one-order of magnitude relative to other less viscous solvents. **IND** and **INR** are a particular group of molecules with N–H···O═C bonds common to the molecule of life, DNA. This makes possible that they share a common origin in Nature.

Supporting Information

Supplementary Figures SI1 to SI31 and Table SI1 are provided as a Source Data File.

CRediT authorship contribution statement

Estefanía Delgado-Pinar : Methodology. **J.Sérgio Seixas de Melo :** Funding acquisition, Supervision.

Declaration of competing interest

The authors declare that they have no known competing financial interests or personal relationships that could have appeared to influence the work reported in this paper.

Data availability

Data will be made available on request.

Acknowledgment

We acknowledge funding by FEDER (Fundo Europeu de Desenvolvimento Regional) through COMPETE (Programa Operacional Factores de Competitividade). The Coimbra Chemistry Centre – Institute of Molecular Sciences (CQC-IMS) is supported by the Fundação para a Ciência e a Tecnologia (FCT), Portuguese Agency for Scientific Research, through Projects UIDB/00313/2020 and UIDP/00313/2020. E.D.-P. thanks FCT "Concurso de Estímulo ao Emprego Científico" for the junior contract CEECIND/04136/2018 and, for Ph.D. Grants, D.C.N. (ref. SFRH/BD/140890/2018) and C.C. (ref. 2020.09661. BD). NMR data collected at the UC-NMR facility are supported in part by the EDRF through the COMPETE Program and by national funds from the FCT through grants RECI/QEQ-QFI/0168/2012 and CENTRO-07-CT62-FEDER-002012, and also through support to Rede Nacional de Ressonância Magnética Nuclear (RNRMN) and to Coimbra Chemistry Centre through grant UID/QUI/00313/2019. Dr. João Pina is acknowledged for the technical help in the fs-TA and fs-UC measurements. CQE is supported by the FCT through project UIDB/00100/2020 e UIDP/00100/2020 and IMS through - LA/P/0056/2020.

Appendix A. Supplementary data

Supplementary data to this article can be found online at https://doi.org/10.1016/j.dyepig.2023.111116.

References

[1] Seixas de Melo J.S. The molecules of colour. The real blue indigo: photostability mechanisms, new functional derivatives, and hybrids. The Royal Society of Chemistry. Photochemistry 2022;49:31–52.
[2] Seixas de Melo J.S. The molecules of colour and Art. Molecules with history and modern applications. In: Albini A, Protti S, editors. Photochemistry. London: The Royal Society of Chemistry; 2020. p. 196–216.
[3] Seixas de Melo J.S. The molecules of colour. In: Albini A, Fasani E, Protti S, editors. Photochemistry. London: The Royal Society of Chemistry; 2018. p. 68–100.
[4] Melo M.J, Ferreira J.L, Parola A.J, Seixas de Melo J.S. Photochemistry for cultural heritage. In: Bergamini G, Silvi S, editors. Applied photochemistry: when light meets molecules. Cham: Springer International Publishing; 2016. p. 499–530.
[5] Melo M.J, Araujo R, Castro R, Casanova C. Colour degradation in medieval manuscripts. Microchem J 2016;124:837–44.
[6] Sousa M.M, Miguel C, Rodrigues I, Parola A.J, Pina F, Seixas de Melo J.S, et al. A photochemical study on the blue dye indigo: from solution to ancient Andean textiles. Photochem Photobiol Sci 2008;7:1353–9.
[7] Dittmann M, Graupner F.F, Maerz B, Oesterling S, de Vivie-Riedle R, Zinth W, et al. Photostability of 4,4′-dihydroxythioindigo, a mimetic of indigo. Angew Chem Int Ed Engl 2014;53(2):591–4.
[8] Moreno M, Ortiz-Sanchez J.M, Gelabert R, Lluch J.M. A theoretical study of the photochemistry of indigo in its neutral and dianionic (leucoindigo) forms. Phys Chem Chem Phys 2013;15(46):20236–46.
[9] Solís Correa H, Ortiz E, Uc V.H, Barceló Quintal I.D, Hernández Avila J.L. Indigo stability: an ab initio study. Mol Simulat 2011;37(13):1085–90.
[10] Correa H.S, Ortiz E, Uc V.H, Quintal I.D.B, Avila J.L.H. Indigo stability: an ab initio study. Mol Simulat 2011;37(13):1085–90.
[11] Iwakura I, Yabushita A, Kobayashi T. Why is indigo photostable over extremely long periods? Chem Lett 2009;38(11):1020–1.
[12] Olivier D, Poincelot M.-A, Douillard S, Lefevre C, Moureau J, Ferandin Y, et al. Photoreactivity of indirubin derivatives. Photochem Photobiol Sci 2008;7(3):328–36.
[13] Jurado-Lopez A, Demko O, Clark R.J.H, Jacobs D. Analysis of the palette of a precious 16th century illuminated Turkish manuscript by Raman microscopy. J Raman Spectrosc 2004;35(2):119–24.
[14] Ferreira E.S.B, Hulme A.N, McNab H, Quye A. The natural constituents of historical textile dyes. Chem Soc Rev 2004;33(6):329–36.
[15] Kupferschmidt K. In search of blue. Science 2019;364(6439):424–9.
[16] Skelton H. A colour chemist's history of Western art. Rev Prog Coloration Relat Top 1999;29(1):43–64.
[17] Balfour-Paul J. Indigo. British Museum Press; 1998.
[18] Balfour-Paul J. Indigo in the arab world. London: RoutledgeCurzon; 1997.
[19] Amato I. Bacterial indigo gives the blues to industrial chemists. Science 1991;253(5025):1213.
[20] Meijer L, Shearer J, Bettayed K, Yoan F. Chapter 24: diversity of intracellular mechanisms underlying the anti-tumor properties of indirubins. In: Meijer L, Guyard N, Skaltsounis L.A, Eisenbrand G, editors. Indirubin, the red shade of indigo. Roscoff, France: life in progress editions; 2006. p. 235–46.
[21] Wang L.G, Mencher S.K. Chapter 25: multiple faces of indirubin and its analogues in fighting cancer. In: Meijer L, Guyard N, Skaltsounis L.A, Eisenbrand G, editors.

Indirubin, the red shade of indigo. Roscoff, France: life in progress editions; 2006. p. 247–58.
[22] Yu A.S, Zhao L. Effects of the GSK-3 beta inhibitor (2Z,3E)-6-bromoindirubin-3'-oxime upon ovarian cancer cells. Tumor Biol 2016;37(4):4857–64.
[23] Seixas de Melo J.S, Rondão R, Burrows H.D, Melo M.J, Navaratnam S, Edge R, et al. Spectral and photophysical studies of substituted indigo derivatives in their keto forms. ChemPhysChem 2006;7:2303–11.
[24] Seixas de Melo J, Rondão R, Burrows H.D, Melo M.J, Navaratnam S, Edge R, et al. Photophysics of an indigo derivative (keto and leuco structures) with singular properties. J Phys Chem A 2006;110:13653–61.
[25] Seixas de Melo J, Moura A.P, Melo M.J. Photophysical and spectroscopic studies of indigo derivatives in their keto and leuco forms. J Phys Chem A 2004;108:6975–81.
[26] Ngan V.T, Gopakumar G, Hue T.T, Nguyen M.T. The triplet state of indigo: electronic structure calculations. Chem Phys Lett 2007;449(1–3):11–7.
[27] Seixas de Melo J.S, Serpa C, Burrows H.D, Arnaut L.G. The triplet state of Indigo. Angew Chem Int Ed 2007;46:2094–6.
[28] Pina J, Sarmento D, Accoto M, Gentili P.L, Vaccaro L, Galvão A, et al. Excited-state proton transfer in indigo. J Phys Chem B 2017;121(10):2308–18.
[29] Pinheiro D, Pineiro M, Galvão A.M, Seixas de Melo J.S. Deep in blue with green chemistry: influence of solvent and chain length on the behaviour of N- and N,N′-alkyl indigo derivatives. Chem Sci 2021;12:303–13.
[30] Pinheiro D, Galvão A.M, Pineiro M, Seixas de Melo J.S. Red-purple photochromic indigos from green chemistry: mono-tBOC or di-tBOC N-substituted indigos displaying excited state proton transfer or photoisomerization. J Phys Chem B 2021;125(16):4108–19.
[31] Cui G.L, Thiel W. Nonadiabatic dynamics of a truncated indigo model. Phys Chem Chem Phys 2012;14(35):12378–84.
[32] Volkov V.V, Chelli R, Righini R, Perry C.C. Indigo chromophores and pigments: structure and dynamics. Dyes Pigments 2020;172:107761.
[33] Roy P.P, Shee J, Arsenault E.A, Yoneda Y, Feuling K, Head-Gordon M, et al. Solvent mediated excited state proton transfer in indigo carmine. J Phys Chem Lett 2020;11:4156–62.
[34] Kleinermanns K, Nachtigallová D, de Vries M.S. Excited state dynamics of DNA bases. Int Rev Phys Chem 2013;32(2):308–42.
[35] Schultz T, Samoylova E, Radloff W, Hertel I.V, Sobolewski A.L, Domcke W. Efficient deactivation of a model base pair via excited-state hydrogen transfer. Science 2004;306(5702):1765–8.
[36] Russell G.A, Kaupp G. Reactions of resonance stabilized carbanions. XXXI. Oxidation of carbanions. 4. Oxidation of indoxyl to indigo in basic solution. J Am Chem Soc 1969;91(14):3851–9.
[37] Alkorta I, Elguero J, Dardonville C, Reviriego F, Santa María D, Claramunt R.M, et al. A theoretical and spectroscopic (NMR and IR) study of indirubin in solution and in the solid state. J Phys Org Chem 2020;33(4):e4043.
[38] Hoessel R, Leclerc S, Endicott J.A, Nobel M.E.M, Lawrie A, Tunnah P, et al. Indirubin, the active constituent of a Chinese antileukaemia medicine, inhibits cyclin-dependent kinases. Nat Cell Biol 1999;1(1):60–7.
[39] Leclerc S, Garnier M, Hoessel R, Marko D, Bibb J.A, Snyder G.L, et al. Indirubins inhibit glycogen synthase kinase-3β and CDK5/P25, two protein kinases involved in abnormal tau phosphorylation in alzheimer's disease: a property common to most cyclin-dependent kinase INHIBITORS?*210. J Biol Chem 2001;276(1):251–60.
[40] Sukari M.A, Vernon J.M. Oxidation of indoles with lead tetra-acetate and hydrolysis of 1,2-disubstituted indol-3-yl acetates. 0. Journal of the Chemical Society, Perkin Transactions 1983;1:2219–23.
[41] Pereira R.C, Pontinha A.D.R, Pineiro M, Seixas de Melo J.S. A comprehensive spectral, photophysical and electrochemical study of synthetic water-soluble acridones. A new class of pH and polarity sensitive fluorescent probes. Dyes Pigments 2019;166:203–10.
[42] Snellenburg J.J, Laptenok S, Seger R, Mullen K.M, Van Stokkum I.H.M. Glotaran: a Java-based graphical user interface for the R package TIMP. J Stat Software 2012;49(3):1–22.
[43] Schmidt M.B.K.K, Boatz J.A, Elbert S.T, Gordon M.S, Jensen J.H, Koseki S, et al. General atomic and molecular electronic structure system. J Comput Chem 1993;14(11):1347–63.
[44] Galvão A.M. Theoretical investigation on the fast kinetics mechanism for vibronically activated photochromism in benzopyrans. The role of the conical intersection topology in driving the mode enhanced photoproducts. J Photochem Photobiol, A: Chem 2014;289:66–72.
[45] Dick B, Haas Y, Zilberg S. Locating conical intersections relevant to photochemical reactions. Chem Phys 2008;347(1):65–77.
[46] Klessinger M, Luettke W. THEORETISCHE und SPEKTROSKOPISCHE untersuchungen an indigo-FARBSTOFFEN--II das chromophore system der indigo-FARBSTOFFE. Tetrahedron 1963;19(Suppl. 2):315–35.
[47] Klessinger M. The origin of the color of indigo dyes. Dyes Pigments 1982;3(2–3):235–41.
[48] Rondão R.J, Seixas de Melo J.S, Schaberle F.B, Voss G. Excited state characterization of a polymeric indigo. Phys Chem Chem Phys 2012;14(5):1778–83.
[49] Horng M.L, Gardecki J.A, Papazyan A, Maroncelli M. Subpicosecond measurements of polar solvation dynamics: coumarin 153 revisited. J Phys Chem 1995;99(48):17311–37.
[50] Nagasawa Y, Taguri R, Matsuda H, Murakami M, Ohama M, Okada T, et al. The effect of hydrogen-bonding on the ultrafast electronic deactivation dynamics of indigo carmine. Phys Chem Chem Phys 2004;6(23):5370–8.
[51] Zhu L, Zhou Q, Cao B, Li B, Wang Z, Zhang X, et al. Theoretical reconsideration of the mechanism of the excited state proton transfer of indigo carmine in water. J Mol Liq 2022;347:118365.
[52] He X, Yang F, Li S, He X, Yu A, Chen J, et al. Ultrafast excited-state intermolecular proton transfer in indigo oligomer. J Phys Chem 2019;123(30):6463–71.
[53] Iwakura I, Yabushita A, Kobayashi T. Kinetic isotope effect on the proton-transfer in indigo carmine. Chem Phys Lett 2010;484:354–7.